Lateral Diffusion of Membrane Lipid-Anchored Probes before and after Aggregation of Cell Surface IgE-Receptors†

Paul S. Pyenta,‡,|| Petra Schwille,§,⊥ Watt W. Webb,§ David Holowka,‡ and Barbara Baird*,‡

Department of Chemistry and Chemical Biology, Baker Laboratory and Department of Applied and Engineering Physics, Clark Hall, Cornell University, Ithaca, New York 14853

Received: January 8, 2003; In Final Form: June 27, 2003

Cross-linking of the high-affinity IgE receptor (FcϵRI) by multivalent antigen on mast cells initiates transmembrane signaling by coupling of FcϵRI with the cytoplasmic tyrosine kinase Lyn in coalesced protein−lipid rafts. As part of our ongoing investigation of these membrane-based interactions, we employed fluorescence correlation spectroscopy and fluorescence photobleaching recovery to compare lateral mobilities of representative components: Cy3−IgE−FcϵRI, a transmembrane protein; DiI−C_{16}, an outer leaflet lipid probe with two saturated acyl chains; PM−EGFP, a Lyn analogue anchored to the inner leaflet via the saturated acyl chains palmitate and myristate; and EGFP−GG, a control protein anchored to the inner leaflet via an unsaturated geranylgeranyl chain and an adjacent polybasic amino acid sequence. Interpreting the data with both free diffusion and anomalous subdiffusion models, we find that EGFP−GG diffuses faster than PM−EGFP on average. Both inner leaflet probes are sensitive to day-to-day variation in diffusion properties but typically diffuse faster than DiI−C_{16}, which is faster than the transmembrane receptor Cy3−IgE−FcϵRI. Large-scale cross-linking of Cy3−IgE−FcϵRI markedly decreases the mobility of this receptor, DiI−C_{16}, and PM−EGFP, whereas EGFP−GG mobility changes little. Quantitative parameters derived from the diffusion data characterize the environment of the coalesced protein−lipid rafts in which Lyn interacts with IgE−FcϵRI after antigen cross-linking, and which also concentrate other raft markers such as DiI−C_{16}. Furthermore, the differences of the diffusion properties for DiI−C_{16} compared to PM−EGFP and EGFP−GG are consistent with the view that the nature of rafts differs between the outer and inner leaflets of the plasma membrane.

Introduction

There is increasing appreciation that plasma membrane lipids participate directly in receptor function, and there are increasing efforts to elucidate the mechanisms of this process. Accumulating data refine the view provided by the fluid-mosaic model[1] and reveal the plasma membrane to be a dynamic, heterogeneous milieu, possibly organized with structural components described as fences, corrals, obstacles, domains, and rafts.[2,3] As one manifestation, lateral diffusion properties have been observed to vary from region to region of the membrane.[4,5] Independent techniques to measure diffusion include fluorescence photobleaching recovery (FPR),[6,7] fluorescence correlation spectroscopy (FCS),[8,9] and single particle tracking.[4,10,11] These measurements, interpreted in terms of free (Brownian) or restricted (anomalous) diffusion, provide complementary information.[12,13] FPR and FCS were employed in the present study to investigate physical interactions within cellular plasma membranes that can be related to receptor-mediated transmembrane signaling.

The roles of specialized membrane domains, commonly called lipid rafts, have received considerable attention in the immunological[14] and cell biological[15] literature. In particular, they have been implicated in the initiation of signal transduction by immunoreceptors as demonstrated for the high affinity receptor (FcϵRI) for IgE in mast cells and basophils,[16,17] T cell receptors,[18,19] and B cell receptors.[20] In the mast cell system, IgE−FcϵRI cross-linking by antigen on the cell surface activates a cytoplasmic signaling cascade. This begins with tyrosine phosphorylation of FcϵRI subunits β and γ at immunoreceptor tyrosine-based activation motifs (ITAMs) in cytosolic segments by Lyn, a Src family kinase.[21] The plasma membrane participates in this cell activation by facilitating functional coupling of FcϵRI and Lyn in coalesced lipid rafts.[22,23]

The protein−lipid rafts associated with clusters of IgE−FcϵRI are enriched in saturated phospholipids, sphingolipids, glycosylphosphatidylinositol (GPI)-anchored proteins, and cholesterol, and they are characteristically resistant to solubilization by certain detergents.[24] Lyn is anchored to the inner leaflet of the plasma membrane by two saturated fatty acids, palmitate and myristate, and a large fraction of Lyn co-isolates with rafts.[16] IgE−FcϵRI associates stably with isolated rafts only after they are cross-linked.[17] Similarly, Lyn/IgE−FcϵRI co-redistribution occurs with raft components on intact cells after receptor cross-linking as measured by fluorescence confocal microscopy.[25] Cholesterol has been shown to be required for these redistributions and correspondingly for effective phosphorylation of cross-linked FcϵRI by Lyn.[26]

Despite widespread recognition of the functional importance of protein−lipid rafts, their physical basis remains ill defined.[23,27] Lipid rafts may involve separation between liquid crystalline (i.e., liquid-disordered) and liquid-ordered phases, or they may actually be induced by interaction with protein aggregates.

† Part of the special issue "A. C. Albrecht Memorial Issue".

* Corresponding author. E-mail: bab13@cornell.edu.
‡ Department of Chemistry and Chemical Biology.
§ Department of Applied and Engineering Physics.
|| Current address: Department of Chemistry and Biochemistry, McMurry University, Abilene TX 79697.
⊥ Current address: Experimental Biophysics Group, Max-Planck-Institute for Biophysical Chemistry, Gottingen, Germany.

10.1021/jp030005t CCC: $25.00
Published on Web 08/29/2003

Liquid-ordered phases have gellike ordering of acyl chains but retain some lateral and rotational freedom of motion of these lipids.[28,29] The nature of rafts on the resting cell membrane, the details of their coalescence after FcϵRI cross-linking, the transbilayer coupling that may occur, as well as the functional advantages provided by rafts are all current areas of investigation.

To explore basic interactions between FcϵRI and Lyn that occur in protein−lipid rafts on live cells, we constructed green fluorescent protein (GFP) chimeras in which 20 amino acid sequences from Lyn or K−Ras containing their lipid-modification residues target these constructs to the inner leaflet of the plasma membrane in live RBL−2H3 cells.[30] The 15 carbon, polyunsaturated geranylgeranyl acyl chain of the GG construct (EGFP−GG) proves a useful comparison to the dual saturated acyl chains of PM−EGFP, the Lyn analogue that preferentially associates with protein−lipid rafts.[30] We showed previously that IgE−FcϵRI cross-linking by antigen leads to its rapid immobilization on the surface of RBL cells.[31] The outer leaflet lipid analogue, DiI−C_{16} (1,1′-dihexadecyl-3,3,3,3′-tetramethylindocarbocyanine iodide), which co-redistributes with aggregated IgE−FcϵRI, similarly loses mobility in receptor-rich patches.[32] In the present study, we use FPR and FCS to compare diffusion properties of PM−EGFP, and EGFP−GG with IgE−FcϵRI and DiI−C_{16}. Under conditions of large-scale receptor cross-linking, we find striking differences between the mobilities of the GFP constructs related to their means of anchoring at the inner leaflet. Implications of these results for rafts in the plasma membrane and for IgE−FcϵRI coupling to Lyn are discussed.

Materials and Methods

Cell Lines. Wild-type RBL−2H3 cells were maintained in monolayer culture and harvested 3−5 d after passage.[33] Enhanced green fluorescent protein (EGFP) (CLONTECH Laboratories, Inc., Palo Alto, CA) constructs, palmitate−myristate−EGFP (PM−EGFP), and EGFP−geranylgeranyl (EGFP−GG), were prepared and transfected into RBL−2H3 cells as described previously.[30] The 20 amino acid sequences from from Lyn or K−Ras, respectively, contain their lipid modification sites.

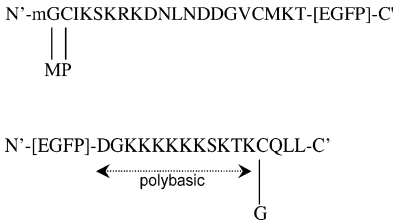

RBL cells expressing the constructs were maintained in culture medium without phenol red and with 500 μg/l Geneticin G418 (Life Technologies, Inc., Rockville, MD) at sub-confluent densities. Both of these stably transfected cell lines were found to be similar to wild-type RBL−2H3 cells in their degranulation response to antigen as measured by β-hexosaminidase release[33] (data not shown).

Labeling with Antibodies and other Reagents. Mouse monoclonal anti-DNP IgE was purified[34] and modified[33] with either Cy3 (Amersham Pharmacia Biotech, Inc., Piscataway, NJ) or Oregon Green (Molecular Probes, Inc., Eugene, OR) using procedures described previously.[30] The dye/IgE stoichiometry was determined to be 6 to 9 by absorption spectroscopy. The labeled IgE were shown to be monomeric by (1) HPLC gel permeation chromatography profiles and (2) their incapacity to trigger degranulation in RBL−2H3 cells in the absence of antigen.

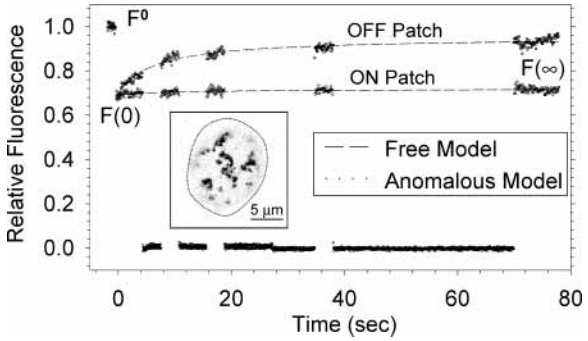

Figure 1. Representative FPR curves of Cy3-IgE−Fc(RI on RBL cells with fits for both free diffusion of a "mobile fraction" (D, f) (eqs 1−6) and anomalous subdiffusion (Γ, α) (eqs 7−10). The fluorescence before bleach ($F°$), the fluorescence just after bleach ($F(0)$), and the fluorescence after a long recovery time ($F(\infty)$) are indicated. Cy3-IgE−sensitized cells were incubated with anti-IgE (10 μg/mL) for 1 h at 4 °C. The curves show fluorescence recovery when the bleached spot is located either off (□) or on (○) a patch. The monitor beam was shuttered intermittently to minimize bleaching. Parameters for the nonlinear least-squares fits to each model are below (nd, not determined). Inset: confocal fluorescence micrograph of RBL cell with patched receptors; the approximate cell boundary is indicated by the dashed line.

	D ($\times 10^{-10}$ cm2/s)	f (%)	Γ ($\times 10^{-10}$ cm2/s$^{\alpha}$)	α
off patch	2.3	84	17	0.6
on patch	nd	9	3.6	0.2

RBL cells were labeled with DiI−C_{16} (Molecular Probes) by incubating with this lipid probe (5 μg/mL from MeOH stock solution of 200 μg/mL) for 1 min at room temperature (22 °C), followed by 10 min at 4 °C. Excess DiI−C_{16} was removed from solution by 3 × sedimentation and resuspension. For IgE sensitization and cross-linking, RBL cells were resuspended at 5×10^6 cells/ml into buffered saline solution (BSS: 135 mM NaCl, 5.0 mM KCl, 1.8 mM $CaCl_2$, 1.0 mM $MgCl_2$, 5.6 mM glucose, 20 mM HEPES) containing 5 mg/mL BSA. IgE was added at 5 μg/mL for 1 h at 37 °C, and cells were then washed by sedimentation and resuspension. IgE−FcϵRI were cross-linked on the cell surface in one of three ways: (1) multivalent antigen DNP−BSA[34] was added at 2 μg/mL for 4 to 6 h at 4 °C; (2) rabbit anti-IgE antibody[32] was added at 10 μg/mL for 4 to 6 h at 4 °C; or (3) biotinylated-anti-ϵ-chain[25] was added at 10 μg/mL for 1 h at 4 °C and after washing, streptavidin was added at 10 μg/mL for 4 to 6 h at 4 °C. The buffer was changed midway to replenish glucose. Incubation in the cold during IgE−FcϵRI aggregation was required to prevent internalization and cellular morphological changes caused by downstream signaling.[25] A shorter incubation of 1 h at 4 °C was sufficient to produce visible patches of labeled IgE−FcϵRI for reliable placement of the FPR laser spot (Figure 1 inset); however, IgE cross-linking incubation for 4 to 6 h was necessary to produce larger patches of IgE−FcϵRI that contain co-redistributed species DiI−C_{16}, PM−EGFP, and EGFP−GG. Figure 1 illustrates how FPR spot placement within or outside a patch reveals distinctive lateral diffusion characteristics.

FPR Measurements. The instrument used for these measurements has been described.[7] Briefly, it consists of a Zeiss Universal microscope with epifluorescence capability (Carl Zeiss, Inc., Thornwood, NY); a 12 W, Coherent Innova 90 argon ion laser (Coherent, Inc., Santa Clara, CA) to serve as a bleaching, monitoring, and wide field light source; a fast shutter system for switching between bleach and monitor beam intensi-

ties; a photomultiplier connected to a SR400 photon counter (Stanford Research Systems, Sunnyvale, CA) to collect fluorescence data; and a desktop computer to control the experiment operation in real time and to analyze the resulting data. The Gaussian profile beam waist (full width, half max) at the focal point using a 100×, 1.3 NA, oil immersion objective is approximately 0.99 and 0.94 μm for the 514 and 488 nm lasing lines, respectively. Spot size was calibrated by measuring monomeric IgE−FcϵRI diffusion on RBL cells and back-calculating assuming $D = 3.0 \times 10^{-10}$ cm^2/s[31,35] as a standard value. The bleach beam is approximately 1000 times more intense than the monitor beam; the bleach duration is typically 5 to 20 ms. The post-bleach monitor beam was collected in 1000 bins of 5 to 100 ms each; the monitor beam was intermittently shuttered about five times during the recovery phase to minimize bleaching of the monitored fluorophore (Figure 1). A 10-μL aliquot of cells was placed on a microscope slide with a #1 coverslip, and the cells were allowed to settle and attach for 5 to 10 min before FPR measurement; no slide was used for more than 15 min.

The free diffusion model is most often used for fitting recovery curves, and assumes random, Brownian-like motion within the membrane.[13,36] Values for parameters $F°$, $F(0)$, and $F(\infty)$, corresponding to pre-bleach intensity, post-bleach intensity, and intensity after a long recovery time, respectively (Figure 1), are calculated using a nonlinear least-squares fit to

$$F(t) = \frac{F(0) + F(\infty)[t/t_{1/2}]}{1 + [t/t_{1/2}]} \tag{1}$$

The half-life $t_{1/2}$ is related to the characteristic diffusion time τ by

$$t_{1/2} = \beta\tau \tag{2}$$

and related to the lateral diffusion coefficient (D) in two-dimensions,

$$r_0^2 = 4D\tau = 4D\frac{t_{1/2}}{\beta} \tag{3}$$

where r_0 is the beam radius at e^{-2} intensity, and β is a calculated parameter that corrects for spot broadening corresponding to bleach depth.[36] The beam radius r_0 is related to the beam waist w (full width, half max) by

$$(2 \ln 2)^{1/2} \cdot r_0 = w \tag{4}$$

We calculate the diffusion coefficient D and the mobile fraction f as

$$D = \beta r_0^2/4t_{1/2} \tag{5}$$

$$f = (F(\infty) - F(0))/(F° - F(0)) \tag{6}$$

An immobile fraction $(1 - f)$ of the fluorescent molecules has customarily been invoked to account for the failure of photobleaching to recover completely. The dashed lines in Figure 1 represent typical fits to the data assuming the free diffusion model.

The anomalous subdiffusion model was used alternatively to analyze fluorescence recovery curves.[13] In this case, the mean square displacement is not assumed to be linear with time as in eq 3, but rather follows

$$\langle x^2 \rangle = 4D(t)t + \Gamma t^\alpha \tag{7}$$

where $0 < \alpha \leq 1$. Correspondingly, the effective diffusion coefficient can be a function of time. $F(\infty)$ is set equal to $F°$ (100% recovery is assumed), and values for the transport coefficient Γ and the time exponent α are extracted. The fitting equation is

$$F(t) = \frac{F(0) + F(\infty)[t/t_{1/2}]^\alpha}{1 + [t/t_{1/2}]^\alpha} \tag{8}$$

The half-life $t_{1/2}$ is related to the characteristic diffusion time as in eq 2, but now

$$r_0^2 = \Gamma\tau^\alpha \tag{9}$$

The transport and diffusion coefficients are related by

$$D(t) = \frac{1}{4}\Gamma t^{\alpha-1} \tag{10}$$

The dotted lines in Figure 1 represent typical fits to the data assuming the anomalous subdiffusion model.

FCS Measurements. The instrument used for these measurements was based on a modified Zeiss IM-35 inverted microscope (Carl Zeiss, Inc., Thornwood, NY) as described.[9] For excitation of EGFP, the 488 nm line of an argon ion laser model 5425 (Ion Laser Technology, Salt Lake City, UT) together with a Nikon 63 × 1.2 NA water immersion objective was used. The back aperture was slightly under-filled creating a diffraction-limited focal spot of approximately 1 μm in diameter. Axial resolution was obtained using a 100-μm multimode optical fiber (OZ optics, Carp, Canada), with the fiber entrance in image plane serving as a confocal pinhole. The fiber was coupled to an avalanche photodiode (EG&G SPCM-200 FC). Suppression of laser light was obtained using a dichroic beam splitter 498/DRLP and band-pass filter HQ530/50 (Chroma Technology, Brattleboro, VT). Cy3 measurements were performed with excitation at 543 nm with HeNe model 1052 laser (Uniphase, San Jose, CA), using a Chroma dichroic 530/DRLP and a D580/50 filter. The detector signal was correlated online by an ALV-5000E board (ALV, Langen, Germany). Excitation power was low (5 μW) for membrane measurements to avoid photobleaching of the fluorophores during the observation time; 30 μW was used for intracellular measurements.

To center the focal spot precisely with about 1 μm diameter and 4 μm height on the membrane, several FCS curves were first taken at different z-positions in 1 μm steps in a representative test cell. The brightness of the fluorescence signal as well as the signal quality of the curve was maximized. Measurements were then taken on cells surrounding the test cell with approximately the same height and thus z-position of the focal spot. Using this procedure, the variation in z-direction was very small ($<1\mu$m).

To determine the relative amount of EGFP derivative located in the membrane compared to that in the cytosol, confocal images were acquired and randomly placed cross-section line profiles were measured (Figure 5b). The profiles were fit with two Gaussian distributions and two flat bases (interior and exterior of the cell) according to the equation

$$F = h \cdot \exp^{-(x-x_1/\sigma_1)^2} + h \cdot \exp^{-(x-x_2/\sigma_2)^2} + \begin{cases} c \text{ if } x_1 < x < x_2 \\ d \text{ if } x < x_1 \text{ or } x > x_2 \end{cases} \tag{11}$$

A single h was used to obtain an average membrane intensity. The exterior base d was subtracted from h and c as background, and the ratio $(h - d)/(c - d)$ was calculated.

Single component, two-dimensional FCS decay curves were fit with the equation

$$G(\tau) = \frac{G(0)}{1 + (t/\tau_D)} \tag{12}$$

where D is defined in eq 3, and $G(0)$ is defined by eq 16. For three-dimensional diffusion, such as cytosolic EGFP, the equation was modified to

$$G(\tau) = \left(\frac{G(0)}{1 + (\tau/\tau_D)}\right) \cdot \left(1 + \left(\frac{r_o}{z_o}\right)^2 \frac{\tau}{\tau_D}\right)^{-1/2} \tag{13}$$

and

$$D = r_0^2/4\tau_D \tag{14}$$

where r_0 and z_0 are the excitation volume dimensions,[37] z_0/r_0 (4 for the FCS apparatus used). For measurements with R independent components (species), eq 12 can be generalized to[38]

$$G(\tau) = \frac{\gamma \sum_{i=1}^{R} a^2{}_i \langle N_i \rangle [1 + (\tau/\tau_{D_i})]^{-1}}{[\sum_{i=1}^{R} a_i \langle N_i \rangle]^2} \tag{15}$$

where a_i and N_i are the relative fluorescence yield and the number density of the ith species, respectively. γ is a parameter relating to the beam geometry; γ (0.5 for a Gaussian profile).[38] Note from eq 15 that $R = 1$ at $\tau = 0$

$$G(0) = \gamma/\langle N \rangle \tag{16}$$

which shows that the FCS autocorrelation extrapolated to the y-axis ($\tau = 0$) is inversely proportional to the number density. We found that as the expression level of PM−EGFP and EGFP−GG varied greatly from cell to cell, and so did $G(0)$ (data not shown). However, because the absolute value of the autocorrelation is arbitrary in relation to the diffusion decay times, data presented (Figures 5 and 6) have been normalized for graphical comparisons.

To be consistent with FPR, the FCS spot size was calibrated by fixing IgE−FcϵRI diffusion coefficient D = 3.0×10^{-10} cm^2/s and back calculating. This value was then used in calculations to determine the diffusion coefficient D for all other species. To avoid photobleaching effects, FCS data were carefully screened to include only those with stable absolute fluorescence intensities over the entire course of the measurement. To test whether the FPR and FCS measurements gave consistent results, RBL cells were labeled with DiI−C_{16}, and aliquots from the same sample were concurrently measured with the two instruments. The measured diffusion coefficients determined by FPR and FCS were within 40% of each other, indicating reasonable agreement between the two methods. There are, however, perturbations of some of the FCS correlation functions for slow membrane diffusion due to residual external noise.

Results

FPR Measurements Without IgE−FcϵRI Cross-Linking. We previously showed that PM−EGFP and EGFP−GG expressed in RBL−2H3 cells target the inner leaflet of the plasma membrane and that they serve as useful models for lipid-anchored cytoplasmic proteins in live cells.[30] PM−EGFP, the Lyn kinase analogue, is anchored by saturated acyl chains C_{14} (myristate) and C_{16} (palmitate). EGFP−GG, the control protein, is anchored by an unsaturated acyl chain C_{15} (geranylgeranylate) and a polybasic amino acid sequence. With FPR measurements, we compared the lateral mobility of these probes to Cy3−IgE bound to FcϵRI, a transmembrane protein, and DiI−C_{16}, a lipid probe in the outer leaflet of the plasma membrane. DiI−C_{16}, added exogenously, has two saturated 16-carbon chains anchoring it to the outer leaflet of the plasma membrane.

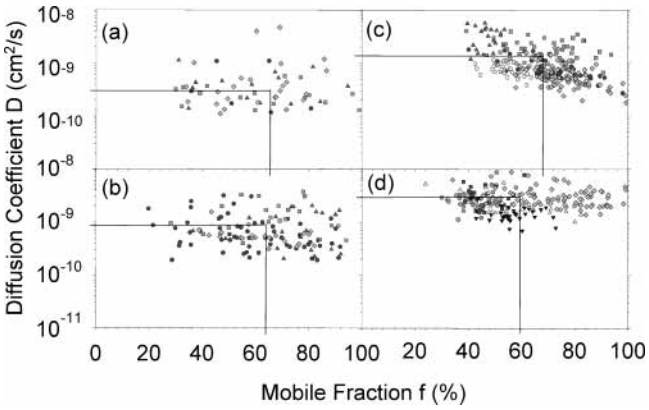

Figure 2. Scatter plots of fitted FPR data in terms of the free-diffusion model (D, f) (eqs 1−6). Except as noted below, cells with indicated probes were maintained at 20 °C without IgE cross-linking. Each point represents a single FPR measurement; different symbols represent identical experimental conditions on different days for the indicated sample. The Cy3−IgE data include monomeric Cy3−IgE−FcϵRI on both control cells and off-patch measurements on cells with cross-linked IgE (incubated at 4°C); these cases were found to be statistically indistinguishable. Numerical means are shown by the horizontal ($\langle D \rangle$) and vertical ($\langle f \rangle$) lines, and these values are included in Table 1 (no cross-linking samples).

Diffusion measurements were made in several independent experiments for Cy3−IgE−FcϵRI on RBL−2H3 cells maintained at 20 °C without IgE cross-linking. Parameters derived from the free diffusion model (eqs 1−6) are plotted in Figure 2a, and data from different days are represented by different symbols. The average mobile fraction (percent recovery) f = 65% is within the range previously reported for fluorescently labeled IgE−FcϵRI on RBL−2H3 cells under similar conditions.[35,39,40] The average diffusion coefficient measured (D = 3×10^{-10} cm^2/sec) is equal to the reference value used for calibration as established previously (Materials and Methods). The (f, D) data points are evenly distributed over the different experiments, and their spread is typical of FPR measurements. Outer leaflet lipid probe, DiI−C_{16}, diffuses several-fold faster than Cy3−IgE−FcϵRI, although it has a similar mobile fraction on average (Figure 2b). Data points for DiI−C_{16} also distribute evenly over different experiments. Parameter averages for Cy3−IgE−FcϵRI and the fluorescent lipid probes are presented in Table 1.

Endogenous PM−EGFP (Figure 2c) and EGFP−GG (Figure 2d) that anchor to the inner leaflet of the bilayer show diffusion characteristics that differ from Cy3−IgE−FcϵRI, DiI−C_{16}, and each other. Although all of the species in Figure 2 have similar mobile fractions on average, the diffusion coefficients for PM−EGFP and EGFP−GG are substantially larger than that for Cy3−IgE−FcϵRI. Averaged over many measurements, both of these lipid-anchored proteins also diffuse significantly faster than DiI−C_{16} in the membrane outer leaflet of these cells (Table 1).

TABLE 1: FPR Parameters for Fluorescent Membrane Probes[a]

probe	n	on/off patch	IgE cross-linking	treatment	D ($\times 10^{-10}$ cm^2/s)	f (%)	Γ ($\times 10^{-10}$ cm^2/s$^\alpha$)	α
Cy3−IgE	77	na	none	20 °C	3.0 ± 0.3	65 ± 3	13 ± 1	0.66 ± 0.04
Cy3−IgE	27	on	DNP−BSA	4 °C, 1−3 hr	nd	18 ± 2	2.3 ± 0.5	0.23 ± 0.03
Cy3−IgE	20	on	αIgE	4 °C, 1−3 hr	nd	22 ± 3	2.9 ± 0.6	0.25 ± 0.04
DiI−C_{16}	213	na	none	20 °C	8.5 ± 0.6	64 ± 2	18 ± 1	0.56 ± 0.02
DiI−C_{16}	50	off	b-αIgE + sa	4 °C, 4−6 hr	15 ± 1	55 ± 1	32 ± 2	0.47 ± 0.02
DiI−C_{16}	21	on	b-αIgE + sa	4 °C, 4−6 hr	nd	32 ± 1	36 ± 4	0.24 ± 0.02
PM−EGFP	284	na	none	20 °C	12 ± 1	68 ± 1	29 ± 0.6	0.54 ± 0.02
PM−EGFP	31	off	αIgE − b + sa	4 °C, 4−6 hr	6.8 ± 0.5	40 ± 2	14 ± 2	0.45 ± 0.02
PM−EGFP	26	on	αIgE − b + sa	4 °C, 4−6 hr	nd	16 ± 1	5.0 ± 1.0	0.48 ± 0.03
EGFP−GG	249	na	none	20 °C	28 ± 1	59 ± 1	63 ± 5	0.56 ± 0.01
EGFP−GG	10	off	αIgE − b + sa	4 °C, 4−6 hr	18 ± 1	40 ± 2	28 ± 3	0.46 ± 0.03
EGFP−GG	17	on	αIgE − b + sa	4 °C, 4−6 hr	18 ± 1	42 ± 2	22 ± 3	0.45 ± 0.02

[a] Mean values (± standard error) from n measurements are shown for both free diffusion (D, f) (eqs 1−7) and anomalous subdiffusion (Γ, α) (eqs 8−9) models. Free diffusion D values are not accurately determined for f values that are less than 40%. Treatment of samples before FPR measurements are described in the legends of Figures 2−4.

For the inner leaflet probes, the data are not uniformly distributed; they tend to cluster for any given day. This difference suggests the mobilities of these acyl chain anchors are sensitive to the membrane composition, which may depend on a number of factors, such as the number of days after cell passage, or the number of cell passages in continuous culture. Because of this variation, we made daily reference measurements of Cy3−IgE−FcϵRI on cells with no receptor cross-linking.

FPR Measurements after IgE-FcϵRI Cross-Linking. We showed previously that endogenous Lyn co-redistributes with cross-linked IgE−FcϵRI on RBL cells, in coalesced protein−lipid rafts that are clearly discernible with fluorescence microscopy after incubation at 4 °C. These low-temperature conditions inhibit stimulation of actin polymerization that causes segregation of Lyn from cross-linked FcϵRI complexes, which are internalized at higher temperatures.[25] We carried out FPR measurements after incubation under low-temperature conditions to examine membrane structures that result from receptor aggregation, before these structures are altered by stimulated actin polymerization and other consequences of downstream signaling.

FPR experiments examined cells with Cy3-IgE (anti-DNP)-FcϵRI cross-linked by DNP−BSA or by anti-IgE (Figure 1 inset), with the laser beam localized either on or off the resulting Cy3−IgE patches (Figure 3a). Our data are consistent with previous diffusion measurements showing that exogenously cross-linked IgE−FcϵRI engage in immobilizing interactions with other cellular components.[31] Fluorescence recovery off the patch is statistically indistinguishable from the values obtained at 20 °C without cross-linking (average $f = 65\%$, Table 1). However, the mobile fraction for Cy3−IgE−FcϵRI after cross-linking and measured on a visible patch is dramatically decreased (average $f = 20\%$). An accurate value for D could not be obtained for these patched receptors because low mobility greatly diminishes the initial part of the recovery curve evaluated by eq 1.

Aggregation of IgE−FcϵRI into these large patches causes visible co-redistribution of fluorescent probes DiI−C_{16}, PM−EGFP and EGFP−GG into the same regions, but with somewhat more diffuse boundaries.[30,32] We employed cross-linking conditions to form sufficiently large patches of these other membrane probes (microns in diameter) that would ensure accurate FPR laser beam localization on or off. IgE−FcϵRI were aggregated first with biotinylated-anti-ϵ-chain, followed by streptavidin and incubation at 4 °C.[25] Results from FPR measurements of the fluorescent membrane probes on or off their own patches, formed after IgE−FcϵRI had been aggregated in this manner, are presented in Figure 3 and in Table 1.

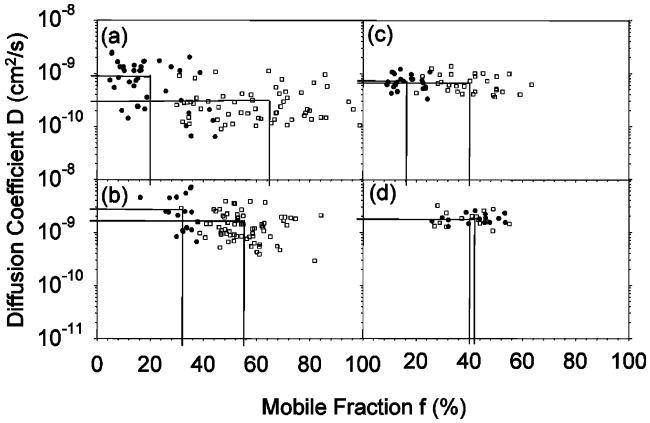

Figure 3. Scatter plots of fitted FPR data for cells with cross-linked IgE−FcϵRI interpreted in terms of the free-diffusion model (D, f) (eq 1−6). Each point represents a single FPR measurement. (a) Cy3−IgE−Fc(RI) were directly aggregated by DNP−BSA (2 μg/mL) or anti-IgE (10 μg/mL) for 1−3 h at 4 °C. For this sample only, the OFF patch designation includes statistically indistinguishable values for monomeric Cy3−IgE−IgE−FcϵRI on non-crosslinked samples (see legend to Figure 2). For DiI−C_{16} (b), PM−EGFP (c), and EGFP−GG (d), IgE−FcϵRI was aggregated with biotinylated anti-IgE and streptavidin for 4−6 h at 4°C. The bleaching spot was positioned either on (●) or off (□) a visible patch of the respective fluorescent probe. Numerical means are shown by the horizontal ($\langle D \rangle$) and vertical ($\langle f \rangle$) lines, and these values are included in Table 1 (cross-linking samples).

In these experiments, DiI−C_{16} behaves similarly to Cy3-IgE when measured on a patch (Figure 3b, Table 1); the mobile fraction decreases from mean values of $f = 55\%$ off a patch to $f = 32\%$ on. Likewise, PM−EGFP shows a marked decrease in these values, from $f = 40\%$ to $f = 16\%$ on a patch. In striking contrast, EGFP−GG shows no significant differences in the f or D values, on or off the patch, suggesting these regions have similar microenvironments for this inner leaflet probe. Because EGFP−GG undergoes significantly less co-redistribution with cross-linked IgE−FcϵRI than does PM−EGFP,[30] measurements of EGFP−GG were limited to a smaller percentage of cells that exhibited apparent patches, and mobility was not detectably reduced in these.

We tested the effects of cold temperature incubation. Parallel FPR measurements were made on cells without and with the 4 to 6 h incubation at 4 °C. When compared directly in 20−40 measurements for each sample, this treatment had very little effect on DiI−C_{16} mobility (without, $f = 76 \pm 2$; with, $f = 74 \pm 3$) or on IgE−FcϵRI mobility (without, $f = 50 \pm 2$; with,

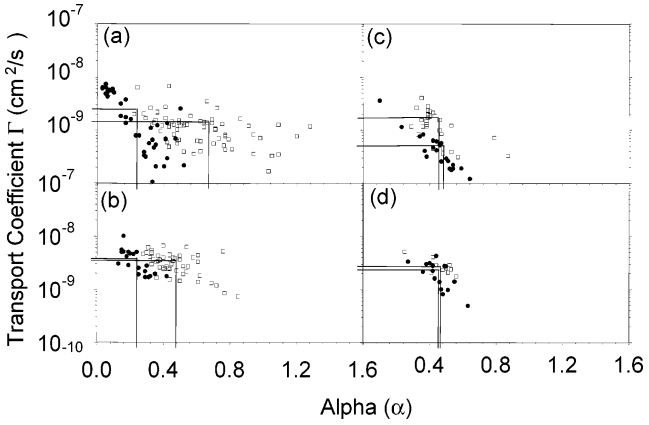

Figure 4. Scatter plots of fitted FPR data for cells with cross-linked IgE−FcϵRI interpreted in terms of the anomalous subdiffusion model (Γ, α) (eqs 7−10). Data are the same as for Figure 3, and conditions are described in that legend: (a) Cy3−IgE−FcϵRI, (b) DiI−C_{16}, (c) PM−EGFP, and (d) EGFP−GG. Each point represents a single FPR measurement. IgE−FcϵRI were directly aggregated, and the bleaching spot was positioned either on (●) or off (□) a visible patch of the respective fluorescent membrane probe. Numerical means are shown by the horizontal ($\langle\Gamma\rangle$) and vertical ($\langle\alpha\rangle$) lines, and these values are included in Table 1 (cross-linking samples).

$f = 55 \pm 2$), but the inner leaflet probes PM−EGFP (without, $f = 72 \pm 2$; with, $f = 57 \pm 3$) and EGFP−GG (without, $f = 70 \pm 2$; with, $f = 61 \pm 2$) both exhibit significantly lower mobile fractions after a long-term cold incubation. Differential sensitivity of the mobile fraction to the cold treatment for these lipid anchored probes is consistent with different environments of the outer and inner membrane leaflets. These results may explain the somewhat lower mobility for off-patch measurements observed for the inner leaflet probes after cross-linking IgE−FcϵRI at 4 °C, but they do not account for the substantially lower values seen for on-patch measurements of PM−EGFP (Table 1).

The FPR measurements on cells without and with IgE−FcϵRI cross-linking were also analyzed within the anomalous subdiffusion framework (eqs 8 and 9), in which D is a function of time and α is the time exponent. These results are presented in Figure 4 and Table 1. As described previously and represented by the curves shown in Figure 1, the two models are not distinguishable from the FPR data but rather provide alternative interpretations.[13] Values for α less than 1 indicate spatial boundaries that restrict the motion. The transport coefficient, Γ, is equal to 4D for $\alpha = 1$ (free diffusion), such that 0.25Γ for $\alpha < 1$ corresponds to D at early times before the spatial boundary is experienced. All four of the membranes probes show $\alpha < 1$, even in the absence of IgE−FcϵRI cross-linking (Table 1), consistent with $f < 1$ for all probes in the free diffusion model. For Cy3−IgE, α for off-patch compared to on-patch shifts downward from 0.66 to 0.24 (Figure 4a). DiI−C_{16} exhibits a similar pattern of increased restriction to diffusion after IgE−FcϵRI is cross-linked; α decreases from 0.47 to 0.24 (Figure 4b). These best fits of the data indicate that, in contrast, PM−EGFP does not change anomalous character (α remains the same) but exhibits a decrease in the average Γ value (Figure 4c). This average could represent more than one subpopulation, including, for example, a very slowly diffusing species that would appear immobile under free diffusion analysis. Neither Γ nor α values for EGFP−GG change appreciably when measured on or off a patch (Figure 4d), corresponding to little change in the f and D values for the two FPR curves.

FCS Measurements. FCS provides an independent method for evaluating probe mobilities, and multi-phasic auto-correlation

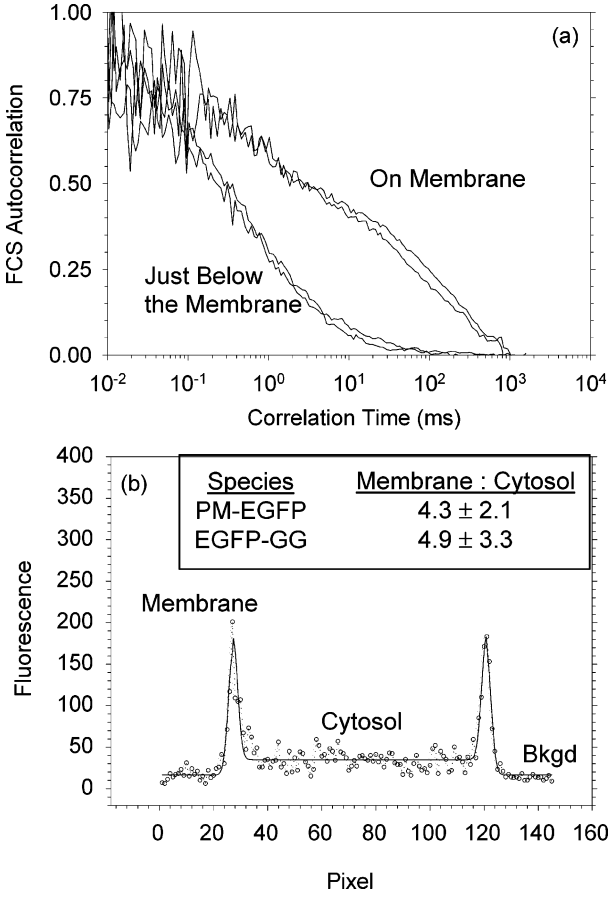

Figure 5. Fluorescence measurements on cells expressing PM−EGFP. (a) Representative FCS autocorrelation curves taken on two different cells to illustrate reproducibility, including possible membrane drift at the longest times. For each cell, excitation volume (height/width ratio $z_0/r_0 = 4$) was focused in the cytosol just below the membrane, and on the plasma membrane. With focus on cytosol, curves exhibit one fast FCS autocorrelation decay time τ_1; with focus on membrane, curves exhibit both a fast τ_1 and a slow τ_2 decay time representing cytosolic and membrane bound populations, respectively. (b) Fluorescence crossline intensity profile from a confocal image of a representative cell. The profile is fit with dual Gaussian distributions (eq 11) and two baselines (solid lines); the ratio of membrane to cytosolic fluorescence is computed after background subtraction. Values for PM−EGFP and EGFP−GG (cell measurement not shown) are given as numerical means (± standard deviations).

curves can reveal coexisting species with different diffusion rates. Within the time frame of this measurement, an immobile population of fluorophores cannot be discerned from background. This complementary approach was utilized to evaluate the membrane probes, including PM−EGFP and EGFP−GG, which are biosynthesized within the cell and transported to the inner leaflet of the plasma membrane. The FCS excitation volume has a height/width ratio (z_0/r_0; eq 13) of approximately 4 [37] and could include contributions to the signal from both cytosolic and membrane bound populations. We found that FCS autocorrelation curves taken while focusing just under the membrane have a single, fast decay time, corresponding to cytosolic GFP. Measurements taken while focusing on the membrane have two decay times, one fast and one slow, corresponding to simultaneous detection of the cytosolic and plasma membrane subpopulations, respectively (Figure 5a).

Most of these inner leaflet probes are expected to go to the membrane, because the dual acylation of PM−EGFP causes a high partition coefficient and a slow off-rate for membrane anchoring. Geranylgeranyl anchoring is also efficient, although

TABLE 2: FCS Parameters for Fluorescent Membrane Probes[a]

probe	n	τ_1 (ms)	τ_2 (ms)	τ_3 (ms)	D_1 ($\times 10^{-10}$ cm^2/s)	D_2 ($\times 10^{-10}$ cm^2/s)	D_3 ($\times 10^{-10}$ cm^2/s)
EGFP	12	0.7 ± 0.01	na	na	440 ± 6	na	na
OG−IgE	5	na	164 ± 5	na	na	3.0 ± 0.09	na
DiI−C_{16}	20	na	150 ± 9	na	na	3.3 ± 0.2	na
PM−EGFP	13	0.7 ± 0.1	119 ± 7	na	480 ± 80	4.2 ± 1.1	na
PM−EGFP−X	5	0.8 ± 0.1	170 ± 30	5100 ± 700	410 ± 50	2.9 ± 0.3	0.09 ± 0.01
EGFP−GG	14	0.9 ± 0.2	61 ± 7	na	360 ± 80	8.1 ± 0.9	na
EGFP−GG−X	7	1.1 ± 0.1	98 ± 7	na	300 ± 30	5.0 ± 0.3	na

[a] Mean values ($\pm$ standard error) from n measurements are shown. τ_1 represents three-dimensional, cytosolic diffusion (eq 13); τ_2 represents two-dimensional, membrane bound diffusion; τ_3 represents two-dimensional, very slow membrane bound diffusion. Values of parameters not required for good fits of the data are designated na. Diffusion coefficients were calculated from corresponding decay times (eq 14). Sample treatments are described in the legend of Figure 6. OG−IgE is IgE covalently labeled with Oregon Green; X indicates samples containing cells with cross-linked IgE−FcϵRI.

less energetically favored than PM;[41] anchoring is enhanced by the polybasic sequence of EGFP−GG. The targeting efficiency of the expressed EGFP constructs to the plasma membrane inner leaflet was evaluated directly with confocal microscopy (e.g., Figure 5b and eq 11). The ratios of label on the membrane to that in the cytosol was determined to be 4.3 for PM−EGFP and 4.9 for and EGFP−GG. These numbers represent lower limits because cellular autofluorescence may contribute to the cytosolic signal. For cell surface FcϵRI labeled exogenously with Cy3-IgE, apparent cytosolic intensity comes only from background and out-of-plane fluorescence. Identical analyses of these images yielded a membrane/cytosol ratio of ~8. To determine which plasma membrane leaflet concentrates the EGFP probes, we used polyclonal-anti-GFP followed secondarily by Cy3-anti-IgG to label cells expressing the constructs after fixation with 4% formaldehyde and permeablization with 0.1% Triton X-100. Confocal images of these cells compared to images of cells similarly treated but excluding the fixation and permeablization steps confirmed PM−EGFP and EGFP−GG to be localized on the membrane inner leaflet (data not shown). The ratio of absolute fluorescence intensities measured with FCS (data not shown) are similar to the cross-section line profiles obtained with confocal microscopy (Figure 5), providing additional support that the fluorescent EGFP constructs are located at the plasma membrane inner leaflet.

All of the plasma membrane probes measured with FPR, and also cytosolic EGFP (no fatty acylation), were measured with FCS in the absence of IgE−FcϵRI cross-linking (Figure 6). The initial, faster component (τ_1) that is present in both PM−EGFP and EGFP−GG decay curves coincides with the single-component decay curve for EGFP, consistent with a cytosolic subpopulation. The second, slower populations of the fatty acylated EGFP probes have decay times (τ_2) consistent with membrane bound species. DiI−C_{16} and IgE−FcϵRI have a single, slower decay time (τ_2), corresponding to their exclusive membrane location. FCS autocorrelation curves from several experiments were fit using eq 12−15. Table 2 compiles these results in terms of characteristic times τ_i and corresponding diffusion coefficients D_i. In this comparison D_2 for IgE−FcϵRI and DiI−C_{16} are similar and somewhat smaller than D_2 for PM−EGFP. The D_2 for EGFP−GG is about 2-fold larger than that for the other membrane probes. These FCS results, and our direct comparison of the FPR and FCS measurements on the same sample (Materials and Methods) are reasonably consistent with the FPR results in Table 1.

Autocorrelation curves for PM−EGFP and EGFP−GG were compared, before and after large-scale cross-linking of IgE−FcϵRI, under conditions similar to those used for the FPR measurements. With the FCS instrumentation, beam location was determined by relative intensity because direct imaging was not possible, as it was for the FPR measurements. Consequently, localization was less certain, and the FCS beam included variable amounts of on- and off-patch regions in the measurements made. For cells expressing PM−EGFP and EGFP−GG, a similarly small reduction in D_2 occurs after the IgE−FcϵRI are aggregated (Table 2). Interestingly, PM−EGFP in cells with cross-linked IgE−FcϵRI consistently exhibited a τ_3 component (Table 2). This may correspond to a very slowly diffusing population that appears immobile in the FPR experiments (Table 1), although other slow processes, such as membrane flow, cannot be ruled out at the present time.

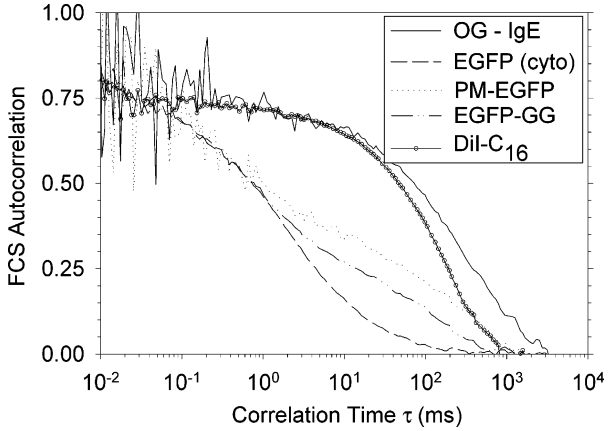

Figure 6. Representative FCS autocorrelation curves for Oregon green−IgE and DiI−C_{16} (two-dimensional diffusion on the cell plasma membrane), PM−EGFP and EGFP−GG (two- and three-dimensional components corresponding to membrane and cytosol, respectively), and cytosolic EGFP (three-dimensional diffusion in the cytosol). Curves have been normalized for direct comparison. Numerical means for the respective decay times (τ) and their corresponding diffusion coefficients (D) are included in Table 2 (no cross-linking samples).

Discussion

This study utilized single cell measurements of lateral diffusion to investigate the membrane environments of IgE−FcϵRI and other components that interact differentially in resting and responding cells. As demonstrated with fluorescence imaging, sucrose gradient analyses, and Western blotting, antigen cross-linking of IgE−FcϵRI causes these cell surface receptors to associate with Lyn in coalesced protein−lipid rafts, resulting in net phosphorylation of FcϵRI cytoplasmic subunits to initiate the signaling cascade.[23] Although the evidence for plasma membrane participation in cellular signaling is increasingly strong, details about the structures and interactions involved remain to be elucidated. Dynamic fluorescence microscopy of GFP analogues of intracellular proteins provide the means to compare the distributions and mobilities in living cells.

The present studies showed with independent methods of FPR and FCS that the membrane environment of a Lyn analogue, PM−EGFP, anchored to the inner leaflet by saturated acyl chains differs significantly from that of EGFP−GG, anchored by an unsaturated acyl chain. Our results are consistent with the view that Lyn preferentially associates with liquid-ordered membrane on intact cells, and the disposition of this changes after IgE−FcϵRI cross-linking.

The diffusion of these lipid-anchored GFP probes on the cytoplasmic side of the plasma membrane inner leaflet could be measured without relying on trans-bilayer transport of amino-containing fluorescent lipid probes[42,43] or on synthetic lipid bilayers with composition similar to the inner leaflet.[44] GFP constructs have enabled other recent studies on inner-leaflet species within intact cells, including diffusion measurements of K−Ras chimeras[45,46] and resonance energy transfer measurements.[47] Because PM−EGFP and EGFP−GG add the GFP component to only 20 amino acid sequences containing the membrane targeting segments, their observed properties are independent of protein interaction motifs, such as the SH2 and SH3 domains of endogenous Lyn.[48] Our diffusion results are consistent with our previous confocal fluorescence imaging and cross-correlation analysis showing that PM−EGFP co-redistributes with cross-linked IgE−FcϵRI,[30] as had been observed for Lyn with immunofluorescence of permeabilized cells.[25] Although EGFP−GG shows some co-redistribution with cross-linked IgE−FcϵRI, this is significantly less and more variable than that for PM−EGFP.[30] Correspondingly, substantially larger changes in diffusion parameters are demonstrated in the current study with PM−EGFP compared to EGFP−GG after IgE−FcϵRI are cross-linked.

FPR Measurements. We compared the plasma membrane diffusion of PM−EGFP and EGFP−GG to Cy−3−IgE−FcϵRI and to DiI−C_{16}, the outer leaflet lipid probe containing two saturated acyl chains. As established previously,[35] external cross-linking of IgE−FcϵRI causes a large reduction in its mobile fraction (Figure 3a), and these immobile complexes are localized in patches of coalesced protein−lipid rafts.[25] If downstream signaling is prevented by reduced temperatures, DiI−C_{16} preferentially co-localizes in these patches, as do Lyn, GPI-linked proteins, and glycosphingolipids.[25] Mobility of DiI−C_{16} is reduced in the IgE−FcϵRI patches (Figure 3b) as previously reported,[32] revealing a local environment that differs from other areas of the membrane.

Despite similar attachment via fatty acid chains, EGFP−GG and PM−EGFP diffuse faster than DiI−C_{16} on resting cells when compared over many measurements (Table 1). These inner leaflet probes also appear more sensitive to daily cellular variations (Figure 2). Faster diffusion of EGFP−GG compared to PM−EGFP probably reflects their tendency to reside in different microenvironments. PM−EGFP behaves similarly to DiI−C_{16} after IgE−FcϵRI is cross-linked; co-localization with the patches[30] is accompanied by reduced mobility (Figure 3c). Because PM−EGFP also co-redistributes with cross-linked outer-leaflet lipid raft components, such as the α-galactosyl ganglioside GD_{1b} and the GPI-linked protein Thy-1,[30] we expect that the PM−EGFP mobility would be reduced in these patches, similar to what was found for DiI−C_{16}. PM−EGFP not associated with the IgE−FcϵRI patches diffuses similarly to PM−EGFP before IgE−FcϵRI cross-linking (Table 1). This population may correspond to Lyn that does not localize with the raft fractions in sucrose gradients[16] and may be dynamically localized to more fluid regions of the plasma membrane.

For EGFP−GG, no decrease in mobile fraction is observed when FPR measurements on patches caused by IgE−FcϵRI cross-linking are compared to off patch measurements. Because EGFP−GG co-redistributes to a lesser extent with the cross-linked IgE−FcϵRI than PM−EGFP and DiI−C_{16},[30] there were fewer clearly identifiable EGFP−GG patches on which to localize the FPR spot. The appearance of some co-redistribution without significant loss of mobility measured by these methods suggests that the polybasic sequence within EGFP−GG contributes to the localization while allowing less constrained diffusion of the unsaturated acyl chain anchor.

The FPR data were also analyzed by the anomalous subdiffusion model (eqs 12 −15; Figure 4) which provides a contrasting view of the diffusing components. As defined in eq 10, the transport coefficient Γ and the time exponential α can be related to an apparent, time-dependent diffusion coefficient $D(t)$.[13] The value $\alpha = 1$ corresponds to free (time-independent) diffusion. For $0 < \alpha < 1$, $D(t)$ decreases during the time interval observed, as if transient confinement points are encountered as the particle diffuses over longer time intervals. The value for Γ corresponds to $4D(t)$ at very early times, before effective boundaries are encountered. For Cy−3−IgE−FcϵRI and DiI−C_{16}, loss of mobility on the patches corresponds to a decreased exponential term α, indicating increased spatial restrictions; Γ remains approximately constant for DiI−C_{16}. This is consistent with expectations from model membrane studies, which showed lateral diffusion in a liquid ordered environment to be only severalfold slower than that in a liquid disordered phase.[49] In contrast, for PM−EGFP, α remains constant, while Γ decreases about 3-fold in the on-patch measurements, suggesting a population of slower-diffusing PM−EGFP located in a liquid ordered domain. EGFP−GG shows no change in Γ or α when compared on or off a patch, consistent with unchanged f and D parameters derived from the free diffusion model.

Overall, the FPR results suggest that the interaction of PM−EGFP with membrane rafts occurs in a different manner than that for DiI−C_{16} or IgE−FcϵRI. This is likely to be due in part to structural differences between the inner and outer leaflets of the plasma membrane. For IgE−FcϵRI, the un-cross-linked complexes are largely in a less ordered lipid environment; cross-linking decreases Γ due to translocation to an ordered protein−lipid environment, and decreases α due to additional structural constraints. DiI−C_{16}, in contrast, may prefer a liquid-ordered environment even in the absence of receptor cross-linking, and this probe appears to experience additional structural constraints as reflected in a decreased value for α, when co-redistributed with IgE−receptor complexes. PM−EGFP (like Lyn itself) at the inner leaflet, is present in both ordered and disordered lipid environments; the lower value of Γ observed for this probe in receptor patches may be due to enrichment in the ordered, raft-associated population, without the additional structural constraints observed for cross-linked IgE−FcϵRI and the outer leaflet component DiI−C_{16}. EGFP−GG, because of its low avidity for the ordered membrane environment,[50] does not exhibit the more restricted diffusion of PM−EGFP.

These results can be compared with those obtained recently with giant unilamellar vesicles of defined lipid mixtures or of lipids derived from the brush border membranes.[51−53] These groups observed large phase-separated lipid domains in register across the bilayer and corresponding several-fold differences in D between these domains for cholesterol-containing membranes.[51,53] Our results indicate that plasma membranes in live cells containing membrane proteins, asymmetry across the bilayer leaflets, and cytoskeletal connections offer additional constraints to those provided by the phase properties of lipids.

FCS Measurements. This complementary method was used to compare the same membrane probes and also unmodified

EGFP located in the cytoplasm (Figure 6). Fluorescent IgE and DiI−C_{16}, added exogenously to the membrane, have a single decay time (τ_2, corresponding to diffusion coefficient D_2; Table 2). PM−EGFP and EGFP−GG, expressed endogenously, have two decay times, corresponding to membrane bound (τ_2, D_2) and cytosolic (τ_1, D_1) populations that are simultaneously observed in FCS measurements, because $z_0/r_0 \sim 4$ (Figure 5a). Consistent with the FPR results, the outer leaflet probe DiI−C_{16} has a smaller D_2 than do the inner leaflet probes, and EGFP−GG has a larger D_2 than does PM−EGFP. FCS measurements for cells with IgE−FcϵRI cross-linked into large patches were more difficult to interpret than the corresponding FPR measurements, because it was not possible to determine where on the plasma membrane the FCS beam was located with respect to the co-redistributed fluorophores. EGFP−GG and PM−EGFP show similar small reductions in D_2 for cells with IgE−FcϵRI cross-linked, indicating effects of this process on the inner leaflet. If a population became immobilized, as suggested by the changing FPR value for f (Table 1), this would not be detected by FCS. Interestingly, FCS curves for EGFP−GG and PM−EGFP were consistently distinguished by the presence for PM−EGFP of an additional decay time, τ_3 (Table 2). This would be consistent with a more slowly diffusing population of PM−EGFP appearing in the cross-linked IgE−FcϵRI patches as suggested by the changing FPR value for Γ (Table 1). However, because of problematic signal/noise ratio in this long time regime, more extensive experiments will be required to obtain an accurate value for τ_3 and to rule out other explanations for this component, such as membrane flow.

In summary, our EGFP constructs provided inner leaflet probes to measure diffusion that is determined by differential anchorage to the plasma membrane. This allowed direct investigation of lipid raft-related interactions. Furthermore, our complementary FPR and FCS measurements and two separate diffusion models revealed features that distinguished the outer leaflet (DiC_{16}) and inner leaflet (PM−EGFP) lipid raft components from the transmembrane receptor (IgE−FcϵRI) that causes their coalescence after receptor cross-linking. In particular, PM−EGFP undergoes a reduction in mobility that may be explained by a slowly diffusing subpopulation within co-redistributed patches of IgE−FcϵRI. This may represent subdomain structures in the inner leaflet with functional relevance. The diffusion properties we observe for PM−EGFP are due to the lipid anchor of Lyn. It will be interesting to see in future experiments how the protein sequences including SH2 and SH3 domains alter their interactions in the early stages of transmembrane signaling initiated by cross-linked IgE−FcϵRI.

Acknowledgment. This project was supported by the National Institutes of Health with research grant RO1 AI18306. Microscopy was carried out in the Biomedical Technology Resource, Developmental Resource for Biophysical Imaging Optoelectronics supported by grant P41-RR04224

References and Notes

(1) Singer, S. J.; Nicolson, G. L. *Science* **1972**, *175*, 720−731.
(2) Edidin, M. *Curr. Opin. Struct. Biol.* **1997**, *7*, 528−32.
(3) Jacobson, K.; Sheets, E. D.; Simson, R. *Science* **1995**, *268*, 1441−1442.
(4) Ghosh, R. N.; Webb, W. W. *Biophys. J.* **1994**, *66*, 1301−1318.
(5) Dietrich, C.; Yang, B.; Fujiwara, T.; Kusumi, A.; Jacobson, K. *Biophys J.* **2002**, *82*, 274−84.
(6) Axelrod, D.; Koppel, D. E.; Schlessinger, J.; Elson, E.; Webb, W. W. *Biophys. J.* **1976**, *16*, 1055−1069.
(7) Thomas, J.; Webb, W. W. In *Noninvasive Techniques in Cell Biology*; Foskett, J. K., Grinstein, S., Eds.; Wiley-Liss: Hoboken, NJ, 1990; 129−152.
(8) Elson, E. L.; Schlessinger, J.; Koppel, D. E.; Axelrod, D.; Webb, W. W. *Prog. Clin. Biol. Res.* **1976**, *9*, 137−47.
(9) Schwille, P.; Korlach, J.; Webb, W. *Cytometry* **1999**, *36*, 176−182.
(10) Barak, L. S.; Webb, W. W. *J. Cell Biol.* **1982**, *95*, 846−52.
(11) Saxton, M. J.; Jacobson, K. *Annu. Rev. Biophys. Biomol. Struct.* **1997**, *26*, 373−399.
(12) Elson, E. L. *Annu. Rev. Phys. Chem.* **1985**, *36*, 379−406.
(13) Feder, T. J.; Brust-Mascher, I.; Slattery, J. P.; Baird, B.; Webb, W. W. *Biophys. J.* **1996**, *70*, 2767−2773.
(14) Micelli, M. C. Lipid Rafts in Immunity, Vol. 13. In *Seminars in Immunology*; Julius, M., Ed.; Academic Press: Orlando, FL, 2001.
(15) Simons, K.; Toomre, D. *Nat. Rev. Mol. Cell Biol.* **2000**, *1*, 31−9.
(16) Field, K. A.; Holowka, D.; Baird, B. *Proc. Natl. Acad. Sci., U.S.A.* **1995**, *92*, 9201−9205.
(17) Field, K. A.; Holowka, D.; Baird, B. *J. Biol. Chem.* **1997**, *272*, 4276−4280.
(18) Xavier, R.; Brennan, T.; Li, Q.; McCormack, C.; Seed, B. *Immunity* **1998**, *8*, 723−32.
(19) Montixi, C.; Langlet, C.; Bernard, A. M.; Thimonier, J.; Dubois, C.; Wurbel, M. A.; Chauvin, J. P.; Pierres, M.; He, H. T. *EMBO J.* **1998**, *17*, 5334−48.
(20) Cheng, P. C.; Dykstra, M. L.; Mitchell, R. N.; Pierce, S. K. *J. Exp. Med.* **1999**, *190*, 1549−60.
(21) Kinet, J.-P. *Annu. Rev. Immunol.* **1999**, *17*, 931−972.
(22) Sheets, E. D.; Holowka, D.; Baird, B. *Curr. Opin. Chem. Biol.* **1999**, *3*, 95−99.
(23) Holowka, D.; Baird, B. *Semin. Immunol.* **2001**, *13*, 99−105.
(24) Brown, D. A.; London, E. *J. Membr. Biol.* **1998**, *164*, 103−114.
(25) Holowka, D.; Sheets, E. D.; Baird, B. *J. Cell Sci.* **2000**, *113*, 1009−19.
(26) Sheets, E. D.; Holowka, D.; Baird, B. *J. Cell Biol.* **1999**, *145*, 877−887.
(27) Brown, D. A.; London, E. *Annu. Rev. Cell Biol.* **1998**, *14*, 111−136.
(28) Schroeder, R. J.; Ahmed, S. N.; Zhu, Y.; London, E.; Brown, D. A. *J. Biol. Chem.* **1998**, *273*, 1150−1157.
(29) Ge, M.; Field, K. A.; Aneja, R.; Holowka, D.; Baird, B.; Freed, J. H. *Biophys. J.* **1999,** *77*, 925−933.
(30) Pyenta, P. S.; Holowka, D.; Baird, B. *Biophys. J.* **2001**, *80*, 2120−32.
(31) Menon, A. K.; Holowka, D.; Webb, W. W.; Baird, B. *J. Cell Biol.* **1986**, *102*, 541−550.
(32) Thomas, J. L.; Holowka, D.; Baird, B.; Webb, W. W. *J. Cell Biol.* **1994**, *125*, 795−802.
(33) Pierini, L.; Holowka, D.; Baird, B. *J. Cell Biol.* **1996**, *134*, 1427−1439.
(34) Posner, R. G.; Lee, B.; Conrad, D. H.; Holowka, D.; Baird, B.; Goldstein, B. *Biochemistry* **1992**, *31*, 5350−5356.
(35) Menon, A. K.; Holowka, D.; Webb, W. W.; Baird, B. *J. Cell Biol.* **1986**, *102*, 534−540.
(36) Yguerabide, J.; Schmidt, J. A.; Yguerabide, E. E. *Biophys. J.* **1982**, *39*, 69−75.
(37) Schwille, P.; Bieschke, J.; Oehlenschläger, F. *Biophys. Chem.* **1997**, *66*, 211−228.
(38) Thompson, N. L. In *Topics in Fluorescence Spectroscopy*; Lakowicz, J. R., Ed.; Plenum Press: New York, 1991; 337−379.
(39) Mao, S.-Y.; Varin-Blank, N.; Edidin, M.; Metzger, H. *J. Immunol.* **1991**, *146*, 958−966.
(40) Posner, R. G.; Subramanian, K.; Goldstein, B.; Thomas, J.; Feder, T.; Holowka, D.; Baird, B. *J. Immunol.* **1995**, *155*, 3601−3609.
(41) Shahinian, S.; Silvius, J. R. *Biochemistry* **1995**, *34*, 3813−3822.
(42) el Hage Chahine, J. M.; Cribier, S.; Devaux, P. F. *Proc. Natl. Acad. Sci. U.S.A.* **1993**, *90*, 447−51.
(43) Morrot, G.; et al. *Proc. Natl. Acad. Sci. U.S.A.* **1986**, *83*, 6863−6867.
(44) Cribier, S.; Morrot, G.; Neumann, J. M.; Devaux, P. F. *Eur. Biophys. J.* **1990**, *18*, 33−41.
(45) Yokoe, H.; Meyer, T. *Nat. Biotechnol.* **1996**, *14*, 1252−6.
(46) Niv, H.; Gutman, O.; Henis, Y. I.; Kloog, Y. *J. Biol. Chem.* **1999**, *274*, 1606−1613.
(47) Zacharias, D. A.; Violin, J. D.; Newton, A. C.; Tsien, R. Y. *Science* **2002**, *296*, 913−6.
(48) Resh, M. D. *Cell. Signal.* **1996**, *8*, 403−412.
(49) Fahey, P. F.; Koppel, D. E.; Barak, L. S.; Wolf, D. E.; Elson, E. L.; Webb, W. W. *Science* **1977**, *195*, 305−306.
(50) Wang, T. Y.; Leventis, R.; Silvius, J. R. *Biochemistry* **2001**, *40*, 13031−40.
(51) Korlach, J.; Schwille, P.; Webb, W. W.; Feigenson, G. W. *Proc. Natl. Acad. Sci. U.S.A.* **1999**, *96*, 8461−6.
(52) Bagatolli, L. A.; Gratton, E. *Biophys. J.* **2000**, *78*, 290−305.
(53) Dietrich, C.; Yang, B.; Fujiwara, T.; Kusumi, A.; Jacobson, K. *Biophys. J.* **2001**, *80*, 1417−28.